PROCEEDINGS OF SCIENCE

ATLAS Pixel Detector: Running Experience

Markus Keil*, **on behalf of the ATLAS Pixel Collaboration**
University of Geneva
E-mail: Markus.Keil@cern.ch

The ATLAS Pixel Detector is the innermost tracking device of the ATLAS experiment. It was successfully commissioned in the year 2008. Calibration measurements have been performed in-situ to set and measure important detector parameters like threshold, charge measurement calibration and timewalk. In combined data taking with the other ATLAS subdetectors by now more than half a million cosmic ray tracks have been collected, which have been used to perform a first detector alignment and to measure pixel hit efficiency and noise occupancy. This paper presents results both from the calibration effort in 2008 and from data taking with cosmic rays. A summary of the current detector status is given.

ATL-INDET-PROC-2009-024
01 December 2009

VERTEX 2009 (18th workshop)
September 13-18 2009
VELUWE, the Netherlands

*Speaker.

1. Introduction

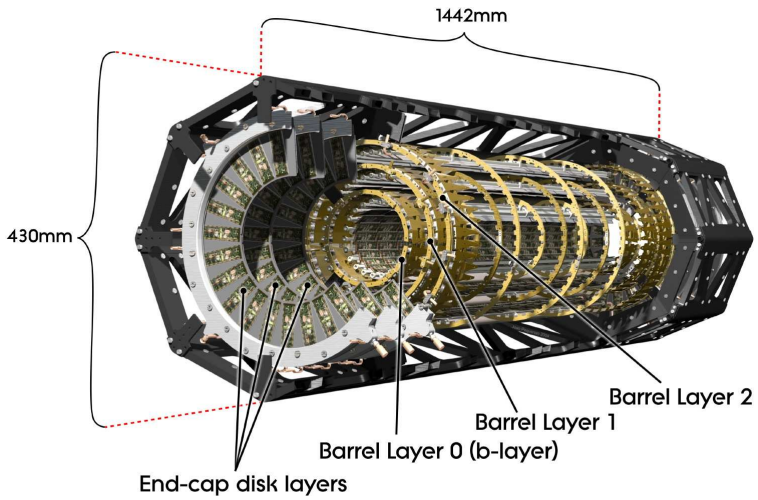

Figure 1: Schematical drawing of the ATLAS Pixel Detector. The detector comprises three barrel layers and two endcaps with three discs each. The single detector modules are mounted on carbon fibre support structures with incorporated cooling circuits.

The ATLAS Pixel Detector [1], shown in Fig. 1, is the innermost tracking detector of the ATLAS experiment. It is made of three concentric barrel layers with mean radii of 50.5 mm, 88.5 mm and 122.5 mm centred around the beam axis and two endcaps with three discs each, forming a three-hit system up to pseudo-rapidities of ± 2.5. The full detector contains 1744 pixel modules, which are mounted on carbon fibre local supports. An evaporative C_3F_8 cooling system is incorporated into the local support to absorb the heat produced by the modules and to allow for an operation at temperatures below 0°C, to limit the effects of radiation damage.

The individual pixel modules (Fig. 2) are made of a 250 μm thick n-on-n silicon sensor, 16 front-end chips and a module controller chip (MCC) [2]. The sensor is divided into 47,232 pixels with a typical pixel size of 50 μm $\times$ 400 μm; approximately 10% of pixels have a size of 50 μm $\times$ 600 μm to bridge the gaps between the readout chips. The sensor is read out by 16 front-end chips with 2880 electronics channels each. Each pixel cell contains a charge sensitive preamplifier, a discriminator and the necessary readout logic to transfer hits to the peripheral logic of the chip, the end-of-column (EOC) logic. In the EOC logic hits are stored up to the programmable trigger latency and sent to the module controller chip (MCC) in case a trigger arrives at the correct latency, erased otherwise. Together with the mere hit location and time, the time-over-threshold (ToT) information is read out for each hit. This is the time interval during which the preamplifier output is above the threshold, in units of the bunch crossing clock (25 ns). Due to the pulse shape of the preamplifier the ToT is a nearly linear function of the deposited charge. Evaluating this ToT information can therefore be used to infer the charge deposited by a passing particle. The routing of signals and power lines of the module is done on the flex hybrid. This is a flexible kapton PCB,

which is glued onto the backplane of the sensor. The connection to the front-end chip is made with wire bonds. The flex hybrid also carries the MCC, which controls the front-end chips and performs an event building with the hit data received from the front-end chips. The off-module connection is provided by a micro cable (type-0 cable), which is either soldered directly onto the flex hybrid (in case of the disc modules) or connected to a kapton pigtail (in case of the barrel module). Figure 2 shows the elements of a pixel barrel module.

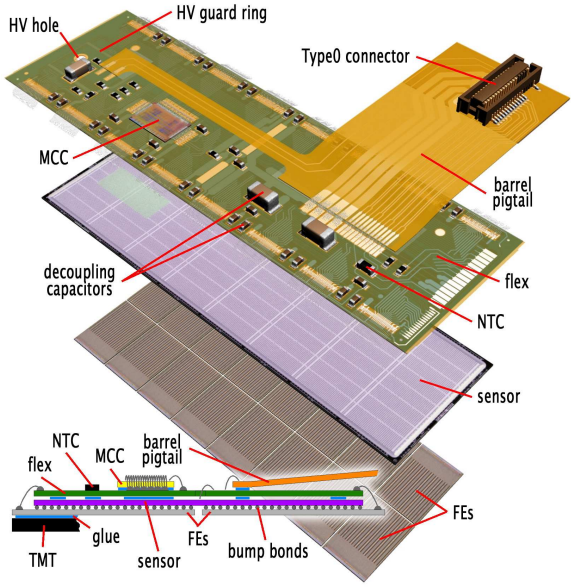

Figure 2: Assembly view and cross section of an ATLAS Pixel Detector module. Sixteen front-end chips are bump bonded to the silicon pixel sensor. Interconnections are done on a flexible kapton PCB, which is connected by wire bonds to the electronics chips.

The transmission of fast signals (data, clock and commands) between the detector and the readout crates in the counting rooms is achieved via optical links. One TTC link per module (Timing, Trigger and Commands) carries the clock and commands to the detector, a data link brings the hit data from the detector to the readout crates. Most modules have one associated data link, only the modules in the innermost barrel layer have two data links per module to accommodate the higher data rate. The electro-optical conversion on the detector side is done on optoboards, which are located at a distance of approximately 1 m from the interaction point.

2. Commissioning and Detector Status

The Pixel Detector was installed and connected inside the ATLAS experiment between summer 2007 and early 2008. The sign-off was foreseen to happen in a two-week period between end of April and beginning of May 2008. However, this period was interrupted by a failure of the evaporative cooling plant. The repairs took several months such that the sign-off had to be finished in an extremely short period at the end of August 2008. In September and October 2008 the Pixel Detector participated in the combined ATLAS data taking with cosmic rays. November and December were used for both detector calibration and cosmic ray data taking. During the LHC

beam injections in early September 2008 the Pixel Detector was put into a safe state, having its high voltage switched off, to protect the electronics from possible beam accidents, which could create a high local charge deposition and thus short-circuit the sensor bias voltage to the readout electronics. The first months of 2009 were used for cooling plant consolidation, operation of the Pixel Detector was resumed in June 2009. The results presented in this paper are from the data taking and calibration in the second half of 2008.

Less than 5% of the modules were not operational during this period due to hardware problems that can either not be repaired or could not be addressed on the short timescale before the initial data taking period in 2008. This includes modules on three leaky cooling loops which were not operated in 2008 as a precautionary measure but are being operated in 2009. Also several modules were connected to faulty off-detector optical components. This was traced back to ESD (electrostatic discharge) problems during the production of the Tx-plugins. All of those plugins have been replaced in the meantime with plugins produced under stricter ESD protection. Only approximately 1.6% of the modules will not be operable due to hardware problems. These remaining problems are mainly due to missing high voltage connections or failures of the on-detector optical components.

3. Calibration

3.1 Optical Link Tuning

The first step in the calibration of the Pixel Detector is establishing the optical communication with the detector modules. Whereas the tuning of the TTC links is straightforward the data links require a more careful adjustment. The main parameters to be adjusted are the sampling threshold and phase of the off-detector receivers for each channel as well as the on-detector laser power. In 2008 97% of the links have been successfully tuned. The knowledge gained has been used to improve the tools used for the tuning such that now basically all links can be tuned in an automatic manner.

3.2 Calibration of the Front-End Electronics

Several parameters of the front-end electronics need to be tuned and calibrated. For this purpose an internal calibration circuit in each front-end chip allows to inject test charges into the preamplifiers and in this way simulate a charge deposition in the sensor with a well defined timing and amount of charge.

The most fundamental electronics parameter of the individual pixel cells is their threshold. The threshold can be adjusted by a 7-bit DAC in each pixel. The individual DAC settings are determined such that the thresholds are as homogenous as possible across the different pixels. After the tuning the threshold and noise values are measured by injecting a varying test charge and measuring the response function for each pixel. This function is best described by an error function, whose 50%-point is identified with the threshold and from whose width the noise value can be determined. Figure 3 (a) shows the threshold distribution for all scanned pixels in the detector. After tuning the threshold distribution has a width of approximately 40 e. The small offset with respect to the target value of 4000 e is due to a bug in the firmware of the readout cards which has been corrected in the

meantime. The noise value obtained from the threshold scan is shown in Fig. 3 (b). For most pixels the noise value is lower than 200 e, some pixels with a different layout in the interchip regions have a higher noise, up to 300 e for the ganged pixels[1]. The tails at high noise values are related to bump bonding problems for a very small number of pixels at the module borders. Figure 4 shows the ratio of threshold-over-noise. For most pixels this ratio is as large as 25, the slightly lower value for the special pixels reflects their larger noise figures.

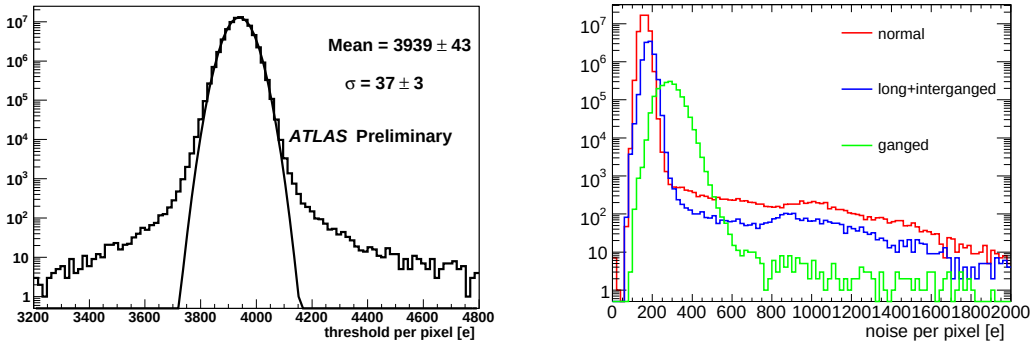

Figure 3: (a) Measured threshold values for all scanned pixels in the detector. The threshold had been tuned to 4000 e before. (b) Noise values obtained from the threshold scan for all scanned pixels in the detector, given by pixel classes.

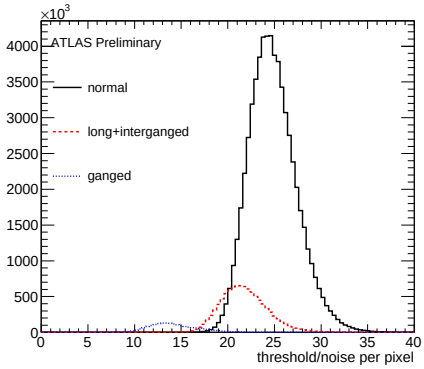

Figure 4: Ratio of threshold over noise for the different pixel classes.

As described before, the time-over-threshold information is stored and read out for all pixel hits. Each single pixel cell contains a 3-bit DAC which allows to adjust the preamplifier feedback current and therefore the ToT behaviour. This is used to achieve a more homogeneous ToT response across all pixels. In the current configuration the ToT behaviour is tuned such that for a charge of 20 ke, corresponding to the most probable charge deposition of one minimum ionising particle in the silicon sensors, a ToT of 30 bunch crossings is obtained.

[1]The electronics cells of these pixels have two sensor pixels connected and therefore a higher capacitive load. For details about the different pixel classes see [2].

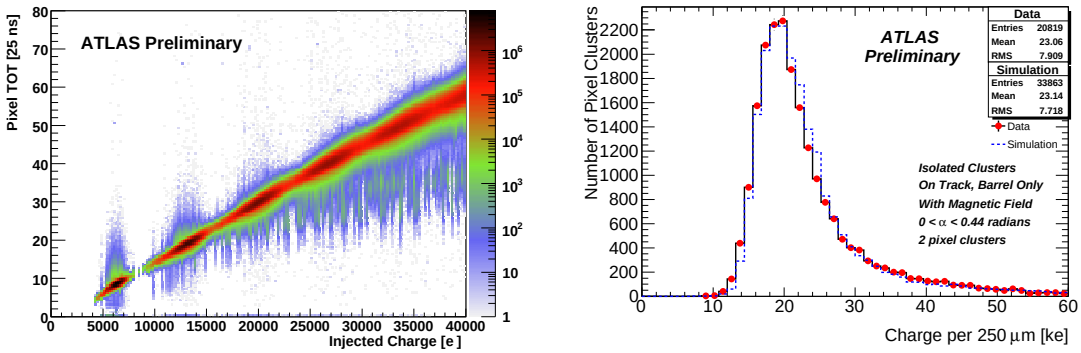

(a) (b)

Figure 5: (a) ToT calibration measurement. The plot shows the measured ToT vs. the injected charge for all scanned pixels in the detector. The ToT has been tuned to a value of 30 for an injected charge of 20 ke. (b) Cluster charge for cosmic ray tracks determined from the ToT information. The measured cluster charges have been normalised to 250 μm path length in the sensor.

In order to be used for the charge measurement the ToT has to be calibrated. This is done with test charge injections, as shown in Fig. 5. The figure shows the measured ToT vs. the injected charge for all scanned pixels in the detector. The measured dependence is fit with an invertible function which can be used to estimate the charge deposition from the ToT of the individual pixel hits. The figure shows that after tuning the vast majority of pixels shows a nearly identical behaviour of ToT vs. charge.

The histogram in Fig. 5 (b) shows the pixel cluster charge for cosmic ray tracks determined from the ToT values. The measured cluster charges have been corrected to a path length of 250 μm in the silicon sensors, using the measured incidence angles of the tracks. The solid line and points represent the data, the dashed line is the distribution predicted by the simulation. One sees a good agreement between the two distributions. The most probable value is close to the expected value of 19,500 e for 250 μm of silicon. This nicely proves the principle of charge measurement by means of the time-over-threshold.

4. Data Taking with Cosmic Rays

Starting from mid-September 2008 the Pixel Detector has been integrated into cosmic ray data taking combined with the other subdetectors. Figure 6 (a) shows the number of tracks for the 2008 data taking period. A total of 270,000 tracks has been collected, 180,000 with and 90,000 without magnetic field. Figure 6 (b) shows the fraction of modules that were enabled during the data taking period. In total more than 95% of the modules were used in the data taking. The main changes in the number of modules occurred at day 20, when the three leaky disc loops where switched off, and at day 70 when a new optolink tuning and the exchange of several off-detector laser plug-ins allowed the recovery of approximately 3% of the modules.

The noise occupancy of the single pixels was determined from data taken with a random trigger. For stable data taking the most noisy pixels were then masked already at the readout stage.

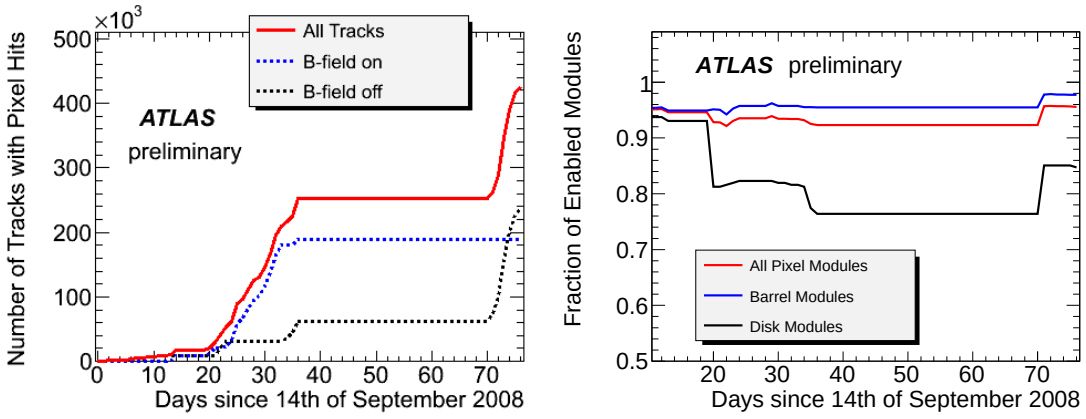

(a) (b)

Figure 6: Statistics of the cosmics data taking in 2008. Plot (a) shows the integrated number of tracks with and without magnetic field, plot (b) shows the fraction of enabled modules. (The fraction is normalised to the respective detector partition, not to the full detector.)

For this purpose an occupancy cut of 10^{-5} hits/pixel/bunchcrossing was applied, resulting in a fraction of $< 10^{-4}$ of masked pixels. The final noise occupancy after the masking of the noisy channels is shown in Fig. 7 (a) for the different detector partitions. In all regions of the detector the noise occupancy is very low, in the order of 10^{-10}.

The events with cosmic ray tracks were then used to measure the hit detection efficiency. This is shown in Fig. 7 (b). The plot shows the measured probability to find a hit in a given barrel layer that matches the coordinates of the extrapolated tracks. This efficiency is approximately 99.8% in all three barrel layers. Due to the spatial distribution of the cosmic ray tracks the hit detection efficiency could not be measured for the endcap discs. Disabled modules were excluded from the calculation.

Apart from measuring the efficiency the cosmic ray tracks were also used to refine the alignment of the Inner Detector. Even though the statistics was not sufficient to perfectly align the detector a very big improvement could be made with respect to the nominal geometry, as measured during production. For the Pixel Detector Fig. 8 shows the residuals, i.e. the difference between the measured and the extrapolated hit position, for the two different pixel directions, using the nominal geometry, the refined alignment and the perfect (simulated) alignment.

Studies of the cluster sizes for tracks with and without magnetic field permitted the measurement of the Lorentz angle of the charge drift inside the silicon sensors. This is shown in Fig. 9 (a). The plot shows the cluster size vs. the track incidence angle (with respect to the normal to the sensor plane) with and without magnetic field. Without magnetic field the cluster size is minimal for perpendicular track incidence (incidence angle 0). With magnetic field this minimum is shifted as the charge carriers do not drift perpendicularly to the sensor plane anymore, but under the Lorentz angle. The average cluster size is therefore minimal when the track angle is equal to the Lorentz angle and the charge carriers drift along the particle track. The measured value of (213.9 ± 0.5) mrad is close to the theoretically expected value of approximately 225 mrad. Figure 9 (b) shows the dependence of the measured Lorentz angle on the temperature of the pixel

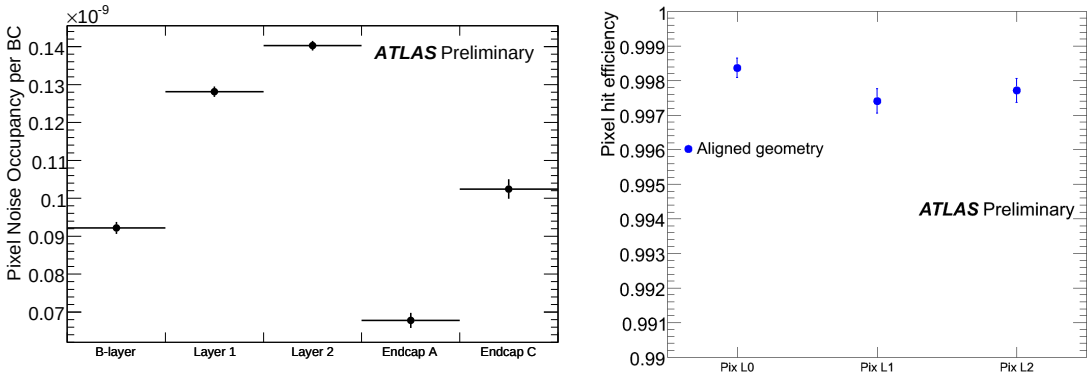

(a) (b)

Figure 7: (a) Pixel occupancy in an event sample without pixel tracks for the three barrel layers and the two endcaps. The noise occupancy after masking the noisiest pixels is approximately 10^{-10}. (b) Efficiency for attaching hits to tracks in cosmic ray data for active modules in the three barrel layers.

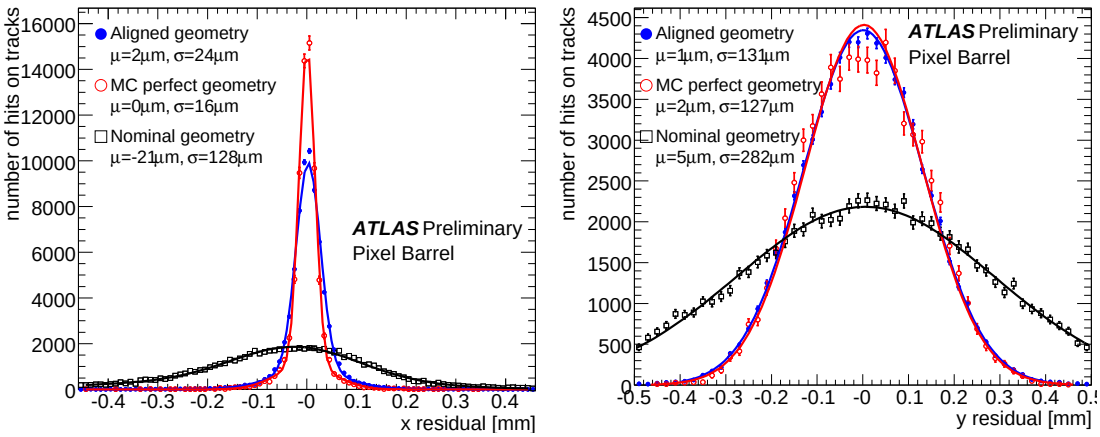

(a) (b)

Figure 8: Unbiased residual distributions, integrated over all hits-on-tracks in the pixel barrel for the nominal geometry and the preliminary aligned geometry. The residual is defined as the measured hit position minus the expected hit position from the track extrapolation. Figure (a) shows the projection onto the local x coordinate, which is the precision coordinate, Figure (b) shows the projection onto the local y coordinate, which is the non-precision coordinate.

module. We see the expected linear dependence, due to the change in the charge carrier mobility. A linear fit yields a value of (-0.78 ± 0.18) mrad/K, which is in agreement with the theoretical expectation of -0.74 mrad/K.

5. Summary

The ATLAS Pixel Detector has been successfully commissioned in 2008. In-situ calibration measurements showed a performance as expected. The electronics thresholds could be tuned to the

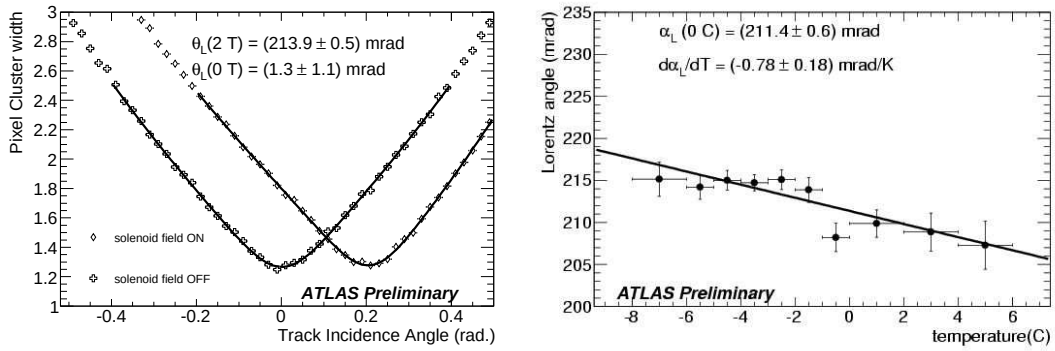

(a) (b)

Figure 9: (a) Cluster size vs. track angle with and without magnetic field. A fit of the curve with magnetic field yields a Lorentz angle of (213.9 ± 0.5) mrad. (b) Measured Lorentz angle vs. the module temperature. The linear fit yields a dependence of (-0.78 ± 0.18) mrad/K.

desired value with a dispersion of approximately 40 e, noise values are below 200 e for standard pixels, slightly higher for some pixels with special layout. The time-over-threshold has proven to be a useful method to measure the deposited charge.

In data taking several hundred thousand cosmic ray tracks have been recorded. Also in the data taking the detector performed well as expected. The noise occupancy is at the level of 10^{-10} with a fraction of 10^{-4} of masked pixels. The efficiency was measured to be 99.8% in the active barrel modules. The alignment could be significantly improved already with cosmic ray data.

The results reported here show that the ATLAS Pixel Detector is ready for data taking with particle collisions, with only 1.6% of disabled modules.

References

[1] ATLAS Pixel Collaboration, ATLAS Pixel Detector Technical Design Report, CERN/LHCC/98-13 (1998).

[2] G. Aad et al., ATLAS Pixel Detector Electronics and Sensors, JINST 3 P07007 (2008).